HHS Public Access

Author manuscript

Oncogene. Author manuscript; available in PMC 2016 October 14.

Published in final edited form as:

Oncogene. 2016 October 13; 35(41): 5350–5361. doi:10.1038/onc.2016.75.

NF-κB-HOTAIR axis links DNA damage response, chemoresistance and cellular senescence in ovarian cancer

Ali R. Özeş[1], **David F. Miller**[2], **Osman N. Özeş**[3], **Fang Fang**[2], **Yunlong Liu**[4,5,6], **Daniela Matei**[6,7,8], **Tim Huang**[9], and **Kenneth P. Nephew**[1,2,6,8,10,*]

[1]Molecular and Cellular Biochemistry Department, Indiana University, Bloomington, IN 47405, USA

[2]Medical Sciences Program, Indiana University School of Medicine, Bloomington, IN 47405, USA

[3]Department of Medical Biology and Genetics, Akdeniz University, Antalya, Turkey

[4]Department of Medical and Molecular Genetics, Indiana University School of Medicine, Indianapolis, Indiana 46202, USA

[5]Center for Computational Biology and Bioinformatics, Indianapolis, Indiana 46202, USA

[6]Indiana University Melvin and Bren Simon Cancer Center, Indianapolis, Indiana 46202, USA

[7]Department of Medicine, Indiana University School of Medicine, Indianapolis, IN 46202, USA

[8]Department of Obstetrics and Gynecology, Indiana University School of Medicine, Indianapolis, IN, 46202, USA

[9]Department of Molecular Medicine/Institute of Biotechnology, The University of Texas Health Science Center at San Antonio, San Antonio, TX, 78229-3900

[10]Department of Cellular and Integrative Physiology, Indiana University School of Medicine, Indianapolis, IN 46202, USA

Abstract

The transcription factor nuclear factor kappa B (NF-κB) and the long non-coding RNA (lncRNA) HOTAIR (HOX transcript antisense RNA) play diverse functional roles in cancer. In this study, we show that upregulation of HOTAIR induced platinum resistance in ovarian cancer, and increased HOTAIR levels were observed in recurrent platinum-resistant ovarian tumors vs. primary ovarian tumors. To investigate the role of HOTAIR during DNA damage induced by platinum, we monitored double-strand breaks and show that HOTAIR expression results in sustained activation of DNA damage response after platinum treatment. We demonstrate that ectopic expression of HOTAIR induces NF-κB activation during DNA damage response and MMP-9 and IL-6 expression, both key NF-κB target genes. We show that HOTAIR regulates activation of NF-κB by

[*]**Corresponding Author:** Kenneth P. Nephew, Ph.D. Professor, Medical Sciences Program, Indiana University School of Medicine, Jordan Hall 302, 1001 E. Third Street, Bloomington, IN 47405-4401, knephew@indiana.edu, Phone: (812) 855-9445.

Conflict of interest

The authors have declared that no conflict of interest exists.

decreasing Iκ-Bα (NF-κB inhibitor) and establish that by inducing prolonged NF-κB activation and expression of NF-κB target genes during DNA damage, HOTAIR plays a critical role in cellular senescence and platinum sensitivity. Our findings suggest that a NF-κB-HOTAIR axis drives a positive-feedback loop cascade during DNA damage response and contributes to cellular senescence and chemotherapy resistance in ovarian and other cancers.

Introduction

The mammalian DNA damage response (DDR) to genotoxic stress is critically important for maintaining genome stability, cell survival and preventing cellular transformation. DDR networks include the classic tumor suppressor gene p53 and its downstream target p21 [1]. More recently, a DDR mechanism has been reported involving nuclear factor kappa B (NF-κB), a master regulator of over 400 genes involved in inflammation, apoptosis, cell cycle control and cell senescence [2, 3]. NF-κB signaling-mediated activation of DDR has been shown to restore genomic integrity, augment cancer cell survival, and play a role in development of resistance to platinum-based cancer therapies [4, 5]. However, distinct DNA damage-induced NF-κB signaling pathways contributing to chemoresistance in cancer have not been well studied.

Platinum, the first line of therapy for ovarian and other cancers, induces inter-and-intra strand crosslinks, generates single stranded breaks and activates nucleotide excision repair [6]. Cellular responses to DNA damage, including response to platinum, can be regulated at the post-transcriptional level by long noncoding RNAs (lncRNAs) [7] . The JADE1 adjacent regulatory RNA (lncRNA-JADE) was reported to play a crucial role in DNA damage-induced, histone H4 acetylation associated with transcriptional activation [8], and lncRNA-p21 was shown to physically interact with hnRNPK (heterogenous nuclear ribonuclear proteins) during DDR and mediate p53-dependent transcriptional repression [9]. Platinum-induced DNA damage resulted in lncRNA PANDA (p21-associated ncRNA DNA damage activated) activation, interaction with transcription factor NF-YA, and PANDA-NF-YA modulation of p53-dependent apoptosis [10].

HOX antisense intergenic RNA (HOTAIR), a lncRNA frequently overexpressed in human cancers [11], was originally identified in 2007 by Rinn et al as a lncRNA located in the HOXC cluster on chromosome 12 that regulates the HOXD gene cluster on chromosome 2 [12]. HOTAIR transcriptionally silences genes located on a distant chromosome region through an epigenetic mechanism involving interaction with polycomb repressive complex 2 (PRC2) [7] . This interaction appears to be required for PRC2 occupancy of specific loci, such as the HOXD locus, trimethylation of histone H3 lysine K27 (H3K27me3) by enhancer of zeste 2 (EZH2) and subsequent gene repression [12, 13]. Additional inter-chromosomal targets of HOTAIR include- cancer-associated genes such as protocadherin (PCDH), ephrin receptor (EPHA1) and the NF-κB inhibitory protein Iκ-Bα [12, 14]. Although epigenetic processes have been reported to play critical roles in DDR [15], including aberrant histone methylation by EZH2 [16, 17], a direct role for HOTAIR in DDR has not been investigated. However, functional overlap between PRC2 and NF-κB activation by genotoxic agents, inflammation, and cancer has been reported [18], suggesting a potential interaction between

NF-κB activation and HOTAIR in response to DNA damage. Furthermore, in solid tumors, including ovarian cancer (OC), enhanced NF-κB activation has been observed in aggressive chemoresistant cell lines [19].

The objective of this study was to investigate the functional role for HOTAIR in DDR and chemotherapy resistance. We demonstrate a strong correlation of HOTAIR overexpression with platinum resistance in OC cell lines and patient tumors. In response to DNA damage, we found that NF-κB directly upregulates HOTAIR expression in OC cell lines. Downregulation of Iκ-Bα during DDR induced a NF-κB-HOTAIR signaling positive-feedback loop cascade, and we demonstrate that DDR further induces HOTAIR-mediated expression of p65-NF-κB and NF-κB target genes MMP9 and IL-6 to promote OC cellular senescence and resistance to DNA-damaging agents. Collectively, these results are the first to demonstrate a role for HOTAIR in DNA damage-induced NF-κB signaling pathway, identifying HOTAIR as a new therapeutic target in drug resistant OC and likely other cancers.

Results

HOTAIR is overexpressed in drug-resistant ovarian cancer

We examined expression of HOTAIR in a panel of OC cell lines (Fig. 1A) representing a spectrum of platinum (CDDP) sensitivity (Resistant; Sensitive). Increased ($P<0.05$) HOTAIR expression was observed in CDDP- resistant (IC_{50} levels >10μM) compared to -sensitive cell lines (Fig. 1A, Supplementary Table S1) and in OC tumors obtained from unpaired patients with CDDP-resistant vs. -sensitive high-grade serous disease (2.1 $\log_2$ fold change; Fig. 1B). We then examined patient data obtained from The Cancer Genome Atlas (TCGA; publically available expression and clinical annotation data) [20]. HOTAIR expression was increased (>0.5 $\log_{10}$ fold-change) in OC patients with recurrent compared to primary high-grade serous disease (Fig. 1C).

Overexpression of HOTAIR increases colony formation and CDDP resistance

To further examine the association between HOTAIR expression and chemoresistance, we either overexpressed (80-fold increase vs. control; Supplementary Fig. S1A) HOTAIR in CDDP-sensitive A2780p or HEYC2 (moderate HOTAIR levels) or knocked-down (70% reduction compared to dsiGFP control, Supplementary Fig. S1B) HOTAIR in CDDP-resistant A2780_CR5 and examined functional changes using clonogenic and proliferation assays *in vitro* and a mouse xenograft model *in vivo*. HOTAIR overexpression increased ($P<0.05$) whereas HOTAIR knockdown decreased ($P<0.05$) OC clonogenic survival (Fig. 1D and Supplementary Fig. S1C). However, overexpression or knockdown of HOTAIR had no effect on cell doubling time (Supplementary Fig. S1D, E), indicating that cell proliferation rate was not altered. To test whether HOTAIR overexpression contributed to CDDP resistance *in vivo*, A2780p were transfected with either HOTAIR or vector control, treated with CDDP or vehicle to induce DNA damage, and then injected subcutaneously in nude mice (see Methods). Tumor size was measured biweekly. Tumor growth, measured by assessing area under the curve (AUC) of the xenograft tumor, was greater ($P<0.05$) for HOTAIR overexpressing OC tumors compared to control (Fig. 1E; Supplementary Fig.

S1F), indicating a role for HOTAIR overexpression in response to DNA damaging agents and CDDP resistance.

HOTAIR mediates DNA damage response (DDR) in ovarian cancer cells

We observed that CDDP treatment of A2780p cells increased ($P<0.05$) HOTAIR expression starting at 16 hr post treatment (Supplementary Fig. S2A) and that HOTAIR expression was also increased by other DNA damage agents mitomycin C and hydrogen peroxide (MMC and H_2O_2; Supplementary Fig. S2B, C). To further examine a role for HOTAIR as a potential mediator of DDR, we examined known cellular responses to genotoxic stress and apoptosis [21] after platinum treatment, including phosphorylation of Chk1 (pChk1), formation of γ-H2AX foci, and caspase cleavage. A2780p cells overexpressing HOTAIR or A2780_CR5 cells transfected with dsiRNA HOTAIR were treated with CDDP. HOTAIR overexpression increased s317 phosphorylation of Chk1, a marker for Chk1 activation, in A2780p (Fig. 2A and Supplementary Fig. S2D), whereas HOTAIR knockdown decreased Chk1 s317 phosphorylation in A2780_CR5 (Fig. 2B and Supplementary Fig. S2E). Interestingly, in the Kuramochi OC cell line harboring p53D281Y mutant (DNA binding mutant), phosphorylation of both p53 and Chk1 was induced by HOTAIR overexpression (Supplementary Fig. S2F). No expression of p21 was observed (data not shown), confirming inactive p53 (Supplementary Table S1). pChk1 levels correlated with γ-H2AX phosphorylation, and the percentage of cells containing >5 γ-H2AX foci increased (1.5 and 4 fold) by 1 and 24 hr of CDDP exposure in HOTAIR overexpressing A2780p cells (Fig. 2C) and decreased in A2780_CR5 cells (2.3 and 1.5 fold) by 1 and 24 hr (Fig. 2D). The number of γ-H2AX foci was unchanged in untreated cells (Supplementary Fig. S2G). Furthermore, enforced overexpression of HOTAIR in A2780p decreased caspase 3/7 cleavage (Fig. 2E; left) and increased caspase 3/7 cleavage in A2780_CR5 cells transfected with dsiRNA HOTAIR (Fig. 2E; right), an established characteristic of cells undergoing apoptosis, indicating that HOTAIR overexpression inhibited platinum-induced apoptosis.

Overexpression of HOTAIR leads to specific changes in gene expression

To investigate the association between HOTAIR, DDR and chemoresistance and identify genes and pathways affected by HOTAIR overexpression, we performed whole transcriptome RNA-sequencing of A2780p (CDDP-sensitive) and A2780_CR5 (CDDP-resistant and endogenous HOTAIR overexpression) OC cell lines. Marked differences in overall gene expression profiles were observed between the paired lines (Supplementary Fig. S3A, B), and expression of DDR-associated genes (e.g., *MLH1* and *XRCC3*), NF-κB pathway (e.g., IL6R, IL4R, NCAM, BCL2L211) and epigenetic regulators (*i.e.*, PRC-associated genes) were prominently altered in A2780_CR5 compared to A2780p (Supplementary Fig. S3C). As expected, differential expression of cancer relevant cellular processes and pathways associated with chemoresistance (anti-apoptotic, cell adhesion, inflammation) in these cell lines was also observed, including the NF-κB pathway (Supplementary Fig. S3B). Further examination of the highly enriched NF-κB pathway by western blot analysis confirmed that total p65 nuclear levels were increased (3.2-fold vs. A2780p) in A2780_CR5 (Fig. 3A).

To validate NF-κB activation by HOTAIR, we measured Iκ-Bα levels in A2780p cells overexpressing HOTAIR treated with CDDP (Fig. 3B). We observed Iκ-Bα protein levels decreased indicating that by repressing the inhibitory Iκ-Bα unit, HOTAIR can activate NF-κB during DDR. Next we measured nuclear p65-NF-κB expression in A2780p HOTAIR overexpressing and A2780_CR5 dsiHOTAIR knockdown cells using immunofluorescence (IF) and western blotting. We observed a 2-fold increase in NF-κB translocation 1 and 24 hr post-CDDP treatment in A2780 cells (Fig. 3C), and an increase in nuclear p65 and decrease in both nuclear and cytoplasmic Iκ-Bα in the western blot (Fig. 3D). Additionally, we observed a 3 and 5 fold decrease in NF-κB translocation 1 and 24 hr post-CDDP treatment in A2780_CR5 cells (Fig. 3E) and a decrease in nuclear p65 and increase in cytoplasmic Iκ-Bα levels with western blotting (Fig. 3F), indicating that HOTAIR expression promotes sustained NF-κB activation during DDR.

To further investigate the role of NF-κB transcriptional activity in stress (genotoxic)-induced HOTAIR expression (Supplementary Fig. 2A, B and C) A2780p cells were treated with CDDP. As shown in Fig. 4A, an increase in HOTAIR expression was observed (9-fold) at 24 hr post-CDDP treatment and co-treatment with an NF-κB inhibitor (Bay-11) inhibited ($P<0.001$) CDDP-induced HOTAIR expression. TNF-α treatment increased ($P<0.05$) expression of HOTAIR (16-fold by 2 hr; Supplementary Fig. 4A) and ectopic overexpression of two known inducers of NF-κB, IKK-α and IKK-β [22], increased ($p<0.05$) HOTAIR expression (3-fold; Fig. 4B). Furthermore, in A2780p ectopically overexpressing HOTAIR, NF-κB targets *IL-6*, and *MMP9* were upregulated ($P<0.05$) while expression of these genes was reduced ($P<0.05$) in HOTAIR knockdown-A2780_CR5 (Fig. 4C). Moreover, in xenograft OC tumors overexpressing HOTAIR, CDDP treatment increased overall expression of HOTAIR and NF-κB target genes, with IL-6 and MMP9 upregulation ($P<0.05$) relative to tumors derived from untreated OC cells (Fig. 4D), confirming functionality of the pathway *in vivo* and stable gene expression changes..

Our findings that HOTAIR expression was increased hours post-DNA damage and this induced expression was blocked by inhibition of NF-κB activation (Supplementary Fig. 2A) indicated transcriptional regulation of the lncRNA in a NF-κB/DNA damage-dependent manner. To begin to determine the underlying mechanism, we used promoter-binding assays to examine the HOTAIR promoter region (1 kb upstream of transcription start site (TSS)). We identified a putative p65-NF-κB binding site (906-GGGACACCCC-915) (Fig. 5A) and investigated NF-κB-p65 binding to the HOTAIR promoter region in A2780_CR5 cells using chromatin immunoprecipitation (ChIP) with five different primer sets (1, 10kb; 2, 8kb, 3, 4kb; 4: 900 bp; 5, 200 bp from the TSS) spanning 10kb upstream of the TSS (Fig. 5B). Enrichment (4-fold) of p65 in the canonical binding site (primers 4 & 5) was observed compared to control primer 1 (Fig. 5B), further supporting a regulatory role for NF-κB pathway in HOTAIR expression. Next, we measured p65-NF-κB binding to the HOTAIR promoter in A2780p cells treated with CDDP in the presence and absence of Bay-11. Enrichment (5.2 fold) of p65 in the canonical binding site 4 was observed compared to control primer (Fig. 5C) and abolished in the presence of Bay-11.

To further examine the transcriptional activation of HOTAIR by p65-NF-κB, transient transfection assays were performed in 293 cells using wild-type or mutant (906-

CTCATTCTCA-915) sequences of HOTAIR promoter along with renilla vector. As shown in Supplementary Fig. S4B, treatment with TNF-α increased ($p<0.05$) luciferase activity (1.6-fold) by the p65-NF-κB wild-type vector, no change in activity of the mutant promoter was observed, and TNF-α-induced luciferase activity was blocked ($P<0.05$) by NF-κB inhibitor Bay-11.

Regulation of HOTAIR expression by NF-κB during DDR

To examine the effect of additional DNA damaging agents on NF-κB activation, we used a previously reported luciferase reporter construct containing 861 base pairs of the E-selectin promoter containing 3 canonical NF-κB-p65-binding sites as a positive control [23]. TNF-α treatment increased luciferase activity compared to empty vector (Supplementary Fig. S4C), confirming luciferase activation by known NF-κB inducers. In cells treated with MMC, H_2O_2 or CDDP, we observed increased luciferase activity, suggesting that various types of DNA damage can activate NF-κB (Supplementary Fig. S4D). To determine NF-kB specific transcription luciferase activity was determined in p65-wt or -mutant vector transfected A2780p cells (described in Supplementary Fig. S4D) treated with MMC, H_2O_2 or CDDP. As shown in Fig. 5D, p65-wt HOTAIR promoter activity was increased by these genotoxic agents (6.9-, 8.2- and 5.0-fold by MMC, CDDP, or H_2O_2 relative to empty vector respectively) and was inhibited ($P<0.05$) by pretreatment with Bay-11 (Fig. 5E). No change in luciferase activity was observed with the p65-mutant construct relative to wild-type vector (Fig. 5D, E). In all, our results suggest that HOTAIR is transcriptionally regulated by NF-κB as a response to DNA damage.

Overexpression of HOTAIR induces IL-6 secretion, DDR activation and cellular senescence

Cytokines in the microenvironment contribute to DNA damage resistance [24] and secretion of cytokines during persistent DNA damage has been reported [25]. IL-6 secretion in particular was shown to contribute to a “chemoresistant niche” [26]. Having observed significant expression of interleukin receptors in A2780_CR5 (Fig. 3B), indicative of pathway activation, we performed an NF-κB target cytokine screen. HOTAIR overexpression was associated with increased (>2-fold) secretion of CCL5, IL-5, IL-6, CXCL-11 and IL-23 compared to vector control (Supplementary Fig. S5A). Moreover, treatment of A2780p cells with “HOTAIR-conditioned” media increased ($P<0.05$) CDDP IC_{50} by >2-fold, which was reversed using an IL-6 neutralizing antibody (Fig. 6A). The addition of recombinant IL-6 to unconditioned media resulted in an approximate 2-fold increase ($P<0.05$) in the IC_{50} for CDDP (Fig. 6B), and dsiRNA knockdown of HOTAIR in A2780_CR5 cells reduced ($P<0.05$) IL-6 secretion (Fig. 6C) and IC_{50} for CDDP (Fig. 6D). Recombinant IL-5 had no effect on CDDP IC_{50} (Supplementary Fig. S5B), further indicating a role for HOTAIR-mediated IL-6 induction in platinum-DNA damage response.

Based on a recent report that unresolved DNA strand breaks (DSBs) caused by DNA damage followed by NF-κB activation and IL-6 secretion can induce cellular senescence [25], we examined whether treatment with low (1μM CDDP or $1/10^{th}$ of IC_{50}) or high (20μM CDDP or 2X the IC_{50}) doses of CDDP induce senescence in A2780p cells overexpressing HOTAIR or not. Activation of p53 and p21 by HOTAIR was observed only during high CDDP treatment, indicated by p53 phosphorylation and p21 expression (Fig.

6E). In addition, IL-6 secretion, an established marker for cell senescence [25, 27], was increased ($P<0.05$) by CDDP in A2780p overexpressing HOTAIR compared to vector transfected cells (Supplementary Fig. S5C). Based on the observation that addition of recombinant IL-6 increased ($P<0.05$) proliferation (Supplementary Fig. S5D), we reasoned that IL-6 secretion by senescent cells induced proliferation of neighboring cells.

We then investigated whether increase in p-Chk1 and p-p53 was dependent on ATR signaling (ataxia telangiectasia mutated (ATM) and Rad3-related (ATR) signaling pathway) [28]. In HOTAIR overexpressing vs. vector control cells, decreased p-p53 levels (Fig. 7A, left) was observed and the level of p-Chk1 was essentially unchanged (Fig. 7A, right), suggesting ATR-dependent activation of p53 by HOTAIR (further supported by no change in proliferation in the presence of ATRi; Supplementary Fig. S5E). Next, we measured p-Chk1 and p-p53 levels in A2780_CR5 cells upon dsiRNA knockdown HOTAIR and observed decreased p-Chk1 and p-p53 levels overall, and this effect was abolished in the presence of ATR inhibitor (Supplementary Fig. S5F). To examine lack of p65-NF-kB on cell proliferation and CDDP-resistance, we stably knocked down p65-NF-kB and validated reduced luciferase activity after stimulation with TNF-α (Supplementary Fig. S6A, B). Interestingly, ectopic expression of HOTAIR in NF-κB knockdown cells rescued ($P<0.05$) proliferation and increased ($P<0.05$) clonogenic survival (Supplementary Fig. S6C, D), which may be attributed to the previously described role of HOTAIR in inhibiting p21 as a potential mechanism of chemotherapy resistance and evasion of apoptosis [29, 30].

To examine cellular senescence, we measured β-galactosidase activity (SA-β-Gal) [31]. In HOTAIR overexpressing A2780p cells, SA-β-Gal positive cell numbers were increased ($P<0.05$) by high vs. low levels of CDDP (Supplementary Fig. S7A), and NF-κB inhibitor Bay-11 reduced ($P<0.05$) the number of senescent cells (Fig. 7B), which is likely a cytostatic effect of the drug (and not cytotoxicity), based on the observation that ectopic expression of HOTAIR increased cell proliferation in cells treated with the NF-κB inhibitor (Supplementary Fig. S5C). DsiRNA knockdown of HOTAIR in A2780_CR5 cells reduced the number of senescent cells (Fig. 7C). Next, we performed flow cytometry in both HOTAIR expressing A2780p and dsiHOTAIR knockdown A2780_CR5 cells 24 and 48 hr post CDDP treatment. We observe a decrease in S1 and an increase in G2 phase 48 hr post CDDP treatment in HOTAIR expressing cells (Fig. 7D) and a reversal of this effect in A2780_CR5 cells (Fig. 7E) suggesting that a subpopulation of cells undergo HOTAIR-dependent cell senescence. Collectively, these results indicate that HOTAIR-induced NF-κB activation and IL-6 secretion contributes to a senescent phenotype, and IL-6 secretion influences the surrounding cell population in a paracrine manner, contributing to chemoresistance (Supplementary Fig. S7C).

Discussion

HOTAIR is a lncRNA frequently overexpressed in solid tumors [32] and associated with cancer cell growth and migration. Although HOTAIR overexpression in OC correlates with disease metastasis and poor patient prognosis [12, 33, 34], the underlying mechanism of HOTAIR upregulation and the role of this important lncRNA in drug resistance in OC and other cancers is not fully understood. In this study, we demonstrate a key role for HOTAIR

in DNA damage: HOTAIR modulates expression of genes activated during DDR, including Chk1 and the levels of γ-H2AX, to inhibit cell cycle progression. Our findings include that HOTAIR activation of the NF-κB pathway following CDDP-induced DNA damage contributes to cellular senescence. Furthermore, we demonstrate that DDR activation of NF-κB induces HOTAIR and a positive feedback loop, resulting in sustained NF-κB activation and persistent DNA damage signaling. As platinum-based regimens continue to be the mainstay of treatment for many solid cancers including OC [35], HOTAIR may represent a target for therapeutic intervention of drug resistance.

Previous mapping studies revealed HOTAIR binding to chromosomal regions near the Iκ-Bα gene, supporting the potential regulation of NF-κB activity by HOTAIR. NF-κB is a master regulator of several cellular responses, including DDR, stress, senescence and inflammation, although its role in cancer is paradoxical, including both oncogenic and tumor suppressive activities [36]. In ovarian and other cancers, NF-κB activation is associated with chemoresistance [37, 38] and activation during DNA damage induced by genotoxic agents has been demonstrated but not well defined [4, 5]. We show that HOTAIR expression modulated NF-κB activation as well as multiple NF-κB target genes including IL-6 and MMP-9 *in vitro* as well as *in vivo*. Consistent with these results, overexpression of HOTAIR increased nuclear translocation of NF-κB, which correlated with reduced total Iκ-Bα levels after CDDP treatment, and HOTAIR overexpression resulted in sustained DDR and NF-κB activation.

Our results also link HOTAIR-mediated IL-6 secretion with platinum resistance (Fig. 6A). The IL-6 cytokine induces apoptosis inhibitors BCL-2, BCL-XL and XIAP and contributes to CDDP-resistance [39]. Importantly, IL-6 secretion has also been linked with exposure to genotoxic stress caused by cisplatin and carboplatin [40]. IL-6 is generally considered a pro-survival cytokine, but sustained IL-6 secretion after DNA damage is linked with cellular senescence [36]. The notion of cell senescence (a tumor suppressor mechanism) contributing to chemotherapy resistance (involves cell proliferation) is an emerging concept. Recent reports suggest that a senescent cell can become a “pro-inflammatory cell” and promote tumor progression by acquiring a senescence associated secretory phenotype (SASP) offer support for this concept [41, 42]. Our findings that HOTAIR can activate NF-kB and its target genes is supported by a recent report implicating HOTAIR in driving the expression of genes directly involved in SASP in urothelial carcinoma, further potentiating an important role for HOTAIR during senescence [43]. Furthermore, it is now strongly believed that the secretion of IL-6 by senescent cells can alter the tumor microenvironment in a paracrine fashion, activating multiple pathways, including the epithelial to mesenchymal transition (EMT) [44], and transforming surrounding stromal cells to a more chemoresistant phenotype [25, 26] (Supplementary Fig. S7B). Our findings on HOTAIR, IL-6, and DNA damage-induced cell senescence are consistent with previous reports associating HOTAIR expression with EMT [33, 34], suggesting promotion of EMT by HOTAIR during chemotherapy-induced DNA damage may contribute to chemoresistance. The slow tumor growth we observed in CDDP-treated HOTAIR expressing cells (Supplementary Fig. S1F) could be attributed to senescent cells altering the microenvironment to a tumor promoting environment, although further studies are needed.

Unresolved DSBs generated by prolonged CDDP-induced DNA damage can result in constitutive activation of DDR signaling and activation of stress response pathways, including senescence [45]. Senescence following irreparable DNA damage has been reported [25], and we investigated whether exposure to low or high dose CDDP would be analogous to early response (transient period) or development of resistance (prolonged period). We demonstrate that prolonged expression of HOTAIR results in γ-H2AX foci formation and subsequent activation of Chk1, which plays a pivotal role during DDR by inducing S15 phosphorylation of tumor suppressor p53 (trans activation domain). The finding that HOTAIR-induced p53 phosphorylation during high CDDP (prolonged exposure) is further supported by the observed induction of p21 (Fig. 6D), a p53 target gene and CDK inhibitor, a process that is ATR-dependent (Supplementary Fig.S7B). As induction of p21 has been closely linked to senescence [46], our findings are the first to indicate a role for HOTAIR in both senescence and chemoresistance. In support of our data, HOTAIR has recently been shown to induce the senescence pathway by its induction of p21 and p15 as well as genes involved in the NF-kB pathway [43, 47]. We posit that HOTAIR can contribute to the activation of several pathways that ultimately lead to chemoresistance. In high DNA damaging conditions a subset of cells can undergo HOTAIR dependent senescence, and at lower or non-senescent conditions HOTAIR can cause resistance in a cell-autonomous manner.

In addition to demonstrating that the above scenario is a NF-κB pathway dependent process, our results indicate that sustained NF-κB activation in HOTAIR expressing cells is due to suppression of Iκ-Bα expression by HOTAIR, in agreement with a previous report linking NF-κB activation to cellular senescence [2]. Recent studies show prolonged NF-κB activation in mutant p53 cells increases inflammation and tumorigenesis, primarily by mutant p53 sequestering tumor suppressor DAB2IP in the cytoplasm [48, 49]. Our observation that HOTAIR induced phosphorylation of mutant p53 (Supplementary Fig. S2C) may provide a mechanistic link for this complex process and support a role for HOTAIR in tumorigenesis in p53 mutant OC, the most commonly mutated gene in the high-grade serous disease [20]. In addition, it is possible that DNA damage can induce a physical interaction between NF-κB and PRC2, which can alter regulation of genes involved during senescence, such as an EZH2-NF-κB interaction [18].

Collectively, our data suggest a model (Fig. S7B) of NF-κB-driven transcription of HOTAIR, which subsequently activates persistent NF-κB expression, IL-6 secretion, and activation of CHK1-p53-p21 pathway, and establishment of a senescence, chemoresistant cancer phenotype. Although the involvement of other NF-κB and HOTAIR target genes in development of chemoresistance cannot be overlooked, the components of this network, including HOTAIR, may represent targets for novel therapeutic strategies to overcome or prevent CDDP-resistance in ovarian and other cancers.

Material and Methods

Cell lines, patient samples, culture conditions and reagents

Epithelial OC cell lines (A2780, A2780_CR5, SKOV3, HEYC2, OV90, IOSE, IGROV, OVMUNA, OV90) were maintained in RPMI 1640 medium (Invitrogen, Carlsbad, CA) as

described previously [50]. Cisplatin-resistant A2780_CR5 was established by continuous exposure to increasing concentrations of cisplatin [50]. Cell lines were authenticated in 2012 by ATCC and tested for mycoplasma contamination (Manassas, VA). High-grade serous ovarian tumors (unpaired samples; chemo-naïve, stage 3–4 or recurrent, platinum resistant), and ovarian surface epithelium (OSE) were surgically collected with informed consent from all subjects (IRB approved protocol IUCRO-0280), snap-frozen, and stored in liquid nitrogen [51]. Cisplatin (CDDP) was purchased from Calbiochem (Billerica, MA), mitomycin C (MMC) was purchased from Sigma Chemical Co. (St. Louis MO), and H_2O_2 was purchased from EMD Millipore (Billerica, MA). NF-κB inhibitor Bay-11–7082 was purchased from Santa Cruz Biotech (Santa Cruz, CA). LZRS-HOTAIR was a gift from Dr. Howard Chang (Stanford University; Addgene plasmid # 26110). Full-length HOTAIR was cloned into pAV5S vector containing a 98-mer aptamer sequence and as a vector control, aptamer cloned into pAV5S was used to account for any possible RNA-dependent signaling effects [52].

Luciferase assays, DNA damage experiments

A2780p cells were seeded in 96-well plates (10^4 cells/well) and transfected with pGL3-promHOTAIR or mutants (500 ng construct/transfection). To normalize transfection efficiency, cells were co-transfected with PGL4 Renilla plasmid (100 ng). Twenty-four hours after transfection, cells were treated with Bay-11–7082 (5ng/mL for 1h) and then TNF-α (10ng/mL), MMC (10μM), CDDP (10μM) or H_2O_2 (10μM) for indicated times and lysed. Luciferase activity was analyzed using the Dual Luciferase Reporter Assay System (Promega, Madison, WI) and a Thermo Scientific Multilabel Plate Reader. To induce DNA damage, cells were treated with CDDP, MMC, H_2O_2 at indicated concentrations and harvested for RNA and protein isolation at the stated time points. Caspase 3/7 cleavage assay was performed according to manufacturers protocol (Caspase 3/7 GloAssay, Promega).

Mutagenesis and RNAi

Site directed mutagenesis was performed with the following forward and reverse primer sets using the QuickChange protocol by Agilent (Santa Clara, CA). Forward primer 5'-GTGGTTTATCTTGCACCCCTCATTCTCAAGCCCCAGCCAGGGAA-3', and reverse primer 5'-TTCCCTGGCTGGGGCTTGAGAATGAGGGGTGCAAGATAAACCAC-3'. The dsiRNA sequences used targeting human HOTAIR (Sense strand 5'-UUCUAAAUCCGUUCCAUUCCACUGCGA-3', and antisense strand 5'-/5Phos/GCAGUGGAAUGGAACGGAUUUAGAA-3') or negative control RNA targeting GFP (Sense strand 5'-CUACAACAGCCACAACGUC-3', and antisense strand 5'-/5Phos/GACGUUGUGGCUGUUGUAG-3'). DsiRNAs were transfected into cells using Lipofectamine 2000 (Invitrogen). shRNA for p65 and control were purchased from Santa Cruz (Sc-29410-SH, and sc-108060). 48 hr post transfection, A2780p cells were selected with 2.5ng/μL puromycin for 5 days and then maintained in 1ng/μL of the drug.

Immunoblot analysis

Cells were lysed in RIPA lysis buffer (50mM Tris-HCl, 150mM NaCl, 1mM EDTA, 1% NP-40, 0.5% sodium deoxycholate and 0.1% SDS) supplemented with protease inhibitors

(Sigma). Protein (approximately 5–10 μg) was loaded on precast 7.5% TGX gels (BioRad, Hercules, CA), blotting was performed as described previously [53] using polyvinylidene difluoride (PVDF) membrane (GE Healthcare, Pittsburg, PA). Membranes were blocked, incubated overnight at 4°C with primary antibody (EZH2, p21, p53, phospho-p53 (S15), β-tubulin, Chk1, phospho-Chk1 (S317), Iκ-Bα, phospho-H2A.X, or Lamin-B (See Supplementary Table S2), washed, and then incubated with HRP-conjugated secondary antibody (Kirkegaard & Perry Laboratories, Gaithersburg, MD), and protein signals were observed using a chemiluminescence system (Thermo Scientific, Schaumberg, IL), according to instructions provided by the manufacturer.

MTT Assay

The quantity of viable cells was calculated by MTT assay as described previously [53]. Absorbance (570 nm; filter reference at 620 nm) was recorded using EnVision Multilabel Plate Reader (Perkin Elmer, Waltham, MA). Doubling time was measured with the equation: duration*log(2)/(log(final concentration)-log(initial concentration)).

RNA extraction and quantitative RT-PCR (qPCR)

RNA was extracted from cell lines and tumors and using RNeasy kit (Qiagen, Venlo, Limburg), cDNA was prepared using MMLV RT system (Promega), and qPCR) was performed with total cDNA and primers for indicated genes and GAPDH or EEF1A as the endogenous control (Supplementary Table S3), using Applied Biosystems 7500 Fast RT-PCR system (Life Technologies, Grand Island, NY) and corresponding software, as we have described [54].

Cytoplasmic and nuclear extractions

Cells were grown to 80% confluence, trypsinized and centrifuged (1200 RPM, 5 min). Cell pellets were washed (1x PBS), re-pelleted (1200 RPM, 5 min), and then lysed in cytoplasmic lysis buffer supplemented with protease inhibitors (10mM Tris-HCl pH 7, 150mM NaCl, 1.5mM $MgCl_2$, 0.5% NP-40; 10 min, 4°C). The lysate was pelleted (1200 RPM, 5 min), the supernatant was used for cytoplasmic buffer, and the remaining pellet was washed (3 times with cytoplasmic lysis buffer, 10 min). After the final wash, the cell pellet was lysed with nuclear lysis buffer (50mM Tris-HCl pH 7, 150mM NaCl, 1.5mM MgCl2, 0.1% SDS, 0.5% sodium deoxycholate, 1% NP-40), the lysate was pelleted (13,000 RPM, 10 min) and the supernatant was used for the nuclear fraction.

Clonogenic survival assay

Cells were seeded ($3–5 \times 10^5$ cells/well) and then transfected with expression vectors for HOTAIR or vector alone (10μg) 24 hrs after seeding using Turbofect (Thermo). At 24 hr post-transfection, cells were treated with CDDP for 3 hrs, washed, serially diluted, plated in triplicate into 6 well plates, allowed 6–8 days of cell growth for colony formation, stained with 5% crystal violet, and cell count was normalized to untreated control as described [54].

Mouse xenograft experiments

All animal studies adhered to ethical regulations and protocols approved by the Institutional Animal Care and Use Committee of Indiana University. To assess tumorigenicity of cells overexpressing HOTAIR, A2780p cells were transfected with pAV5S–HOTAIR or pAV5S–aptamer and 24 hr post-transfection cells were treated or not with CDDP for 3 hr, washed with PBS trypsinized and counted with trypan blue, re-suspended in 1:1 PBS/matrigel (BD Bioscience) and injected subcutaneously into the left flank of 3- to 4- week-old female nude athymic mice (BALB/ c-nu/nu; Harlan, Indianapolis, IN), as described [54, 55]. Engrafted mice (4 per group) were inspected three times per week for tumor appearance by visual observation and palpation. Tumor length (l) and width (w) were measured weekly using digital calipers and tumor volume (v) was calculated as $v=½ \times l \times w^2$. No randomization was used and no animals were excluded from the final data. The investigator measuring tumor size was blinded to the treatment groups. Mice were sacrificed when tumor diameter reached 2 cm or at the end of study.

ELISA and cytokine release assays

Conditioned media were prepared by washing culture plates with PBS followed by incubation in serum-free RPMI medium with antibiotics for 48 hr and stored at −80°C. Total cell counts were determined and ELISA was performed using kits and procedures from R&D systems (Minneapolis, MN. Cytokine release assay, Cat #ARY005) and eBiosciences (San Diego, CA. IL-6 ELISA Cat # 88-7066-22). The data were normalized to the cell number and reported as fold change. IL-6 release assay was performed 3 times and the cytokine release assay was performed once.

Immunofluorescence quantification

A2780p cells transfected with HOTAIR expression plasmid or vector control were plated on glass slides (50,000 cells/well), incubated overnight 4°C with anti-phospho-H2AX or anti-p65 antibodies (See Supplementary Table S2), and the number of cells displaying nuclear p65 or γ-H2AX was determined in ten random images from 3 independent experiments using a light microscope (60X magnification). Fluorescence intensity was analyzed using image J software. To determine the difference in intensity, whole cell individual intensities and the nuclear intensity were measured, intensities were averaged and normalized to control to determine fold translocation

ChIP assays

Cells were cross-linked (1% formaldehyde) and dynabeads (Life Technologies) coupled to the appropriate secondary antibody were used to immunoprecipitate sheared chromatin extracts treated with anti-p65. After reversing the crosslinks, DNA was purified, and standard curve of ChIP input DNA was prepared. Enrichment was calculated by using qPCR to compare the level of the target region in each sample to the mean of negative control genomic regions. Primers designed for the specified genomic regions (Integrated DNA Technologies, Coralville, Iowa) amplified a single product from input DNA based on a single melting peak (Supplementary Table S4). Each ChIP DNA sample was assayed for the levels of negative control regions.

Senescence-detection assays

Senescence-associated β-galactosidase was detected in A2780p cells fixed with 5% formaldehyde and incubated in staining solution (Sigma) and 1mg/ml 5-bromo-4-chloro-3-indolyl β-d-galactosidase (X-Gal, Invitrogen), for 24 hr at 37 °C cells, following the protocol of Debacq-Chainiaux [31]. The number of distinct blue cells were counted (20X magnification) and normalized to the total number of cells.

RNA-sequencing analysis of A2780p and A2780_CR5 cells

Stranded whole transcriptome RNA-seq was performed essentially as we have described [56]. Briefly, biological duplicates of A2780p and A2780_CR5 cells (10^7 culture dish) were lysed and RNA was extracted according to manufacturers protocol (Qiagen RNeasy Mini kit). Total RNA was size fractionated by size using ethanol concentration manipulations. The large RNA fraction (>200 nt) was fragmented prior to library construction. Ribosomal RNA was reduced by duplex specific nuclease (DSN) following limited hybridizations of both fractions and then amplified to add barcodes for multiplexing on the Illumina HiSeq2000 platform. Demultiplexing was performed by CASAVA v1.8.2 and trimming was accomplished with Trimmomatic v0.22 with additional trimming by fastx_clipper v0.0.13.2. Read mapping was performed by tophat2 v2.0.6 to the human genome hg19 (UCSC) with Gencode annotation v13 allowing no more than two mismatches. RNA sequencing data can be accessed using SRA number SRP066008.

TCGA Analysis

The IlluminaHiSeq RNASeq data was provided by the Genome Sciences Centre, BCCA. The RPKM values were provided from TCGA database. The exon-exon junction sequences and their corresponding coordinates were defined based on annotations of any transcripts in UCSC known genes, Ensembl (v54) or the Refseq database (as downloaded from the UCSC genome browser on March 2009).

Statistical analysis

All data are presented as mean values ± SD of at least three biological experiments unless otherwise indicated. CDDP IC_{50} values were determined by Prism 6 (GraphPad Software, San Diego, CA), using logarithm normalized sigmoidal dose curve fitting. The estimate variation within each group were similar therefore student's *t*-test was used to statistically analyze the significant difference among different groups by using Prism 4.0 (GraphPad Software). The genome-wide analysis experiments were conducted as described previously[56, 57] using the Partek Genomics Suite (version 6.5).

Supplementary Material

Refer to Web version on PubMed Central for supplementary material.

Acknowledgments

We thank Aaron Buechlein (Indiana University) for help with bioinformatic analysis of TCGA data, Dr. Craig Pikaard (Indian University) for the pAV-spinach vector, Dr. Howard Chang (Stanford University;) for LZRS-HOTAIR vector, and Dr. Heather O'Hagan for carefully reading this manuscript and helpful suggestions. This work

was made possible by funding from the National Cancer Institute (Awards CA13001 and CA182832), Walther Cancer Foundation (Indianapolis, IN), and the Doane and Eunice Dahl Wright Fellowship (Medical Sciences Program, Indiana University, Bloomington, IN).

References

1. Zhang X-P, Liu F, Wang W. Regulation of the DNA damage response by p53 cofactors. Biophysical journal. 2012; 102(10):2251–2260. [PubMed: 22677378]
2. Chien Y, et al. Control of the senescence-associated secretory phenotype by NF-κB promotes senescence and enhances chemosensitivity. Genes & development. 2011; 25(20):2125–2136. [PubMed: 21979375]
3. Wang J, et al. RelA/p65 functions to maintain cellular senescence by regulating genomic stability and DNA repair. EMBO reports. 2009; 10(11):1272–1278. [PubMed: 19779484]
4. Wu Z-H, et al. Molecular linkage between the kinase ATM and NF-κB signaling in response to genotoxic stimuli. Science. 2006; 311(5764):1141–1146. [PubMed: 16497931]
5. Janssens S, et al. PIDD mediates NF-κB activation in response to DNA damage. Cell. 2005; 123(6): 1079–1092. [PubMed: 16360037]
6. Deans AJ, West SC. DNA interstrand crosslink repair and cancer. Nature Reviews Cancer. 2011; 11(7):467–480. [PubMed: 21701511]
7. Guttman M, et al. Chromatin signature reveals over a thousand highly conserved large non-coding RNAs in mammals. Nature. 2009; 458(7235):223–227. [PubMed: 19182780]
8. Wan G, et al. A novel non-coding RNA lncRNA-JADE connects DNA damage signalling to histone H4 acetylation. The EMBO journal. 2013; 32(21):2833–2847. [PubMed: 24097061]
9. Huarte M, et al. A large intergenic noncoding RNA induced by p53 mediates global gene repression in the p53 response. Cell. 2010; 142(3):409–419. [PubMed: 20673990]
10. Hung T, et al. Extensive and coordinated transcription of noncoding RNAs within cell-cycle promoters. Nature genetics. 2011; 43(7):621–629. [PubMed: 21642992]
11. Tsai M-C, Spitale RC, Chang HY. Long intergenic noncoding RNAs: new links in cancer progression. Cancer research. 2011; 71(1):3–7. [PubMed: 21199792]
12. Gupta RA, et al. Long non-coding RNA HOTAIR reprograms chromatin state to promote cancer metastasis. Nature. 2010; 464(7291):1071–1076. [PubMed: 20393566]
13. Guil S, et al. Intronic RNAs mediate EZH2 regulation of epigenetic targets. Nature structural & molecular biology. 2012; 19(7):664–670.
14. Chu C, Qu K, Zhong FL, Artandi SE, Chang HY. Genomic maps of long noncoding RNA occupancy reveal principles of RNA-chromatin interactions. Molecular cell. 2011; 44(4):667–678. [PubMed: 21963238]
15. Balch C, et al. The epigenetics of ovarian cancer drug resistance and resensitization. American journal of obstetrics and gynecology. 2004; 191(5):1552–1572. [PubMed: 15547525]
16. Liu L, et al. miR-101 regulates expression of EZH2 and contributes to progression of and cisplatin resistance in epithelial ovarian cancer. Tumor Biology. 2014:1–8.
17. Hu S, et al. Overexpression of EZH2 contributes to acquired cisplatin resistance in ovarian cancer cells in vitro and in vivo. Cancer biology & therapy. 2010; 10(8):788–795. [PubMed: 20686362]
18. Lee ST, et al. Context-specific regulation of NF-κB target gene expression by EZH2 in breast cancers. Molecular cell. 2011; 43(5):798–810. [PubMed: 21884980]
19. Yang G, et al. The biphasic role of NF-κB in progression and chemoresistance of ovarian cancer. Clinical Cancer Research. 2011; 17(8):2181–2194. [PubMed: 21339307]
20. Network CGAR. Integrated genomic analyses of ovarian carcinoma. Nature. 2011; 474(7353):609–615. [PubMed: 21720365]
21. Ciccia A, Elledge SJ. The DNA damage response: making it safe to play with knives. Molecular cell. 2010; 40(2):179–204. [PubMed: 20965415]
22. Zandi E, et al. The IκB kinase complex (IKK) contains two kinase subunits, IKKα and IKKβ, necessary for IκB phosphorylation and NF-κB activation. Cell. 1997; 91(2):243–252. [PubMed: 9346241]

23. Ozes ON, et al. NF-κB activation by tumour necrosis factor requires the Akt serine-threonine kinase. Nature. 1999; 401(6748):82–85. [PubMed: 10485710]
24. Canino C, et al. SASP mediates chemoresistance and tumor-initiating-activity of mesothelioma cells. Oncogene. 2011; 31(26):3148–3163. [PubMed: 22020330]
25. Rodier F, et al. Persistent DNA damage signalling triggers senescence-associated inflammatory cytokine secretion. Nature cell biology. 2009; 11(8):973–979. [PubMed: 19597488]
26. Gilbert LA, Hemann MT. DNA damage-mediated induction of a chemoresistant niche. Cell. 2010; 143(3):355–366. [PubMed: 21029859]
27. Kuilman T, et al. Oncogene-induced senescence relayed by an interleukin-dependent inflammatory network. Cell. 2008; 133(6):1019–1031. [PubMed: 18555778]
28. Bieging KT, Mello SS, Attardi LD. Unravelling mechanisms of p53-mediated tumour suppression. Nature Reviews Cancer. 2014; 14(5):359–370.
29. Liu Z, et al. The long noncoding RNA HOTAIR contributes to cisplatin resistance of human lung adenocarcinoma cells via downregualtion of p21 (WAF1/CIP1) expression. PLoS One. 2013; 8(10):e77293. [PubMed: 24155936]
30. Jing L, et al. HOTAIR enhanced aggressive biological behaviors and induced radio-resistance via inhibiting p21 in cervical cancer. Tumor Biology. 2014; 36(5):3611–3619. [PubMed: 25547435]
31. Debacq-Chainiaux F, et al. Protocols to detect senescence-associated beta-galactosidase (SA-βgal) activity, a biomarker of senescent cells in culture and in vivo. Nature protocols. 2009; 4(12):1798–1806. [PubMed: 20010931]
32. Malek E, Jagannathan S, Driscoll JJ. Correlation of long non-coding RNA expression with metastasis, drug resistance and clinical outcome in cancer. Oncotarget. 2014; 5(18):8027. [PubMed: 25275300]
33. Wu Z-H, et al. Long non-coding RNA HOTAIR is a powerful predictor of metastasis and poor prognosis and is associated with epithelial-mesenchymal transition in colon cancer. Oncology reports. 2014; 32(1):395–402. [PubMed: 24840737]
34. Qiu, J-j, et al. Overexpression of long non-coding RNA HOTAIR predicts poor patient prognosis and promotes tumor metastasis in epithelial ovarian cancer. Gynecologic oncology. 2014
35. Vaughan S, et al. Rethinking ovarian cancer: recommendations for improving outcomes. Nature Reviews Cancer. 2011; 11(10):719–725. [PubMed: 21941283]
36. de Visser KE, Eichten A, Coussens LM. Paradoxical roles of the immune system during cancer development. Nature reviews cancer. 2006; 6(1):24–37. [PubMed: 16397525]
37. Kipps E, Tan DS, Kaye SB. Meeting the challenge of ascites in ovarian cancer: new avenues for therapy and research. Nature Reviews Cancer. 2013; 13(4):273–282.
38. Almeida LO, et al. NFκB mediates cisplatin resistance through histone modifications in head and neck squamous cell carcinoma (HNSCC). FEBS open bio. 2014; 4:96–104.
39. Wang Y, et al. Autocrine production of interleukin-6 confers cisplatin and paclitaxel resistance in ovarian cancer cells. Cancer letters. 2010; 295(1):110–123. [PubMed: 20236757]
40. Dijkgraaf EM, et al. Chemotherapy alters monocyte differentiation to favor generation of cancer-supporting M2 macrophages in the tumor microenvironment. Cancer research. 2013; 73(8):2480–2492. [PubMed: 23436796]
41. Kang C, et al. The DNA damage response induces inflammation and senescence by inhibiting autophagy of GATA4. Science. 2015; 349(6255):aaa5612. [PubMed: 26404840]
42. Laberge R-M, et al. MTOR regulates the pro-tumorigenic senescence-associated secretory phenotype by promoting IL1A translation. Nature cell biology. 2015; 17(8):1049–1061. [PubMed: 26147250]
43. Heubach J, et al. The long noncoding RNA HOTAIR has tissue and cell type-dependent effects on HOX gene expression and phenotype of urothelial cancer cells. Molecular cancer. 2015; 14(1):108. [PubMed: 25994132]
44. Sullivan N, et al. Interleukin-6 induces an epithelial-mesenchymal transition phenotype in human breast cancer cells. Oncogene. 2009; 28(33):2940–2947. [PubMed: 19581928]

45. Oliver TG, et al. Chronic cisplatin treatment promotes enhanced damage repair and tumor progression in a mouse model of lung cancer. Genes & development. 2010; 24(8):837–852. [PubMed: 20395368]

46. Di Micco R, et al. Oncogene-induced senescence is a DNA damage response triggered by DNA hyper-replication. Nature. 2006; 444(7119):638–642. [PubMed: 17136094]

47. Yoon J-H, et al. Scaffold function of long non-coding RNA HOTAIR in protein ubiquitination. Nature communications. 2013:4.

48. Di Minin G, et al. Mutant p53 Reprograms TNF Signaling in Cancer Cells through Interaction with the Tumor Suppressor DAB2IP. Molecular cell. 2014

49. Cooks T, et al. Mutant p53 prolongs NF-κB activation and promotes chronic inflammation and inflammation-associated colorectal cancer. Cancer cell. 2013; 23(5):634–646. [PubMed: 23680148]

50. Li M, et al. Integrated analysis of DNA methylation and gene expression reveals specific signaling pathways associated with platinum resistance in ovarian cancer. Bmc Medical Genomics. 2009; 2:34. [PubMed: 19505326]

51. Matei D, et al. Epigenetic resensitization to platinum in ovarian cancer. Cancer Res. 2012; 72:2197–2205. [PubMed: 22549947]

52. Paige JS, Wu KY, Jaffrey SR. RNA mimics of green fluorescent protein. Science. 2011; 333(6042): 642–646. [PubMed: 21798953]

53. Rao X, et al. MicroRNA-221/222 confers breast cancer fulvestrant resistance by regulating multiple signaling pathways. Oncogene. 2010; 30(9):1082–1097. [PubMed: 21057537]

54. Wang Y, et al. Epigenetic Targeting of Ovarian Cancer Stem Cells. Cancer research. 2014; 74(17): 4922–4936. [PubMed: 25035395]

55. Zhang S, et al. Identification and characterization of ovarian cancer-initiating cells from primary human tumors. Cancer research. 2008; 68(11):4311–4320. [PubMed: 18519691]

56. Miller DF, et al. A new method for stranded whole transcriptome RNA-seq. Methods. 2013; 63(2): 126–134. [PubMed: 23557989]

57. Miller DF, et al. Stranded Whole Transcriptome RNA-Seq for All RNA Types. Current Protocols in Human Genetics. 2015:11.14. 1–11.14. 23. [PubMed: 25599667]

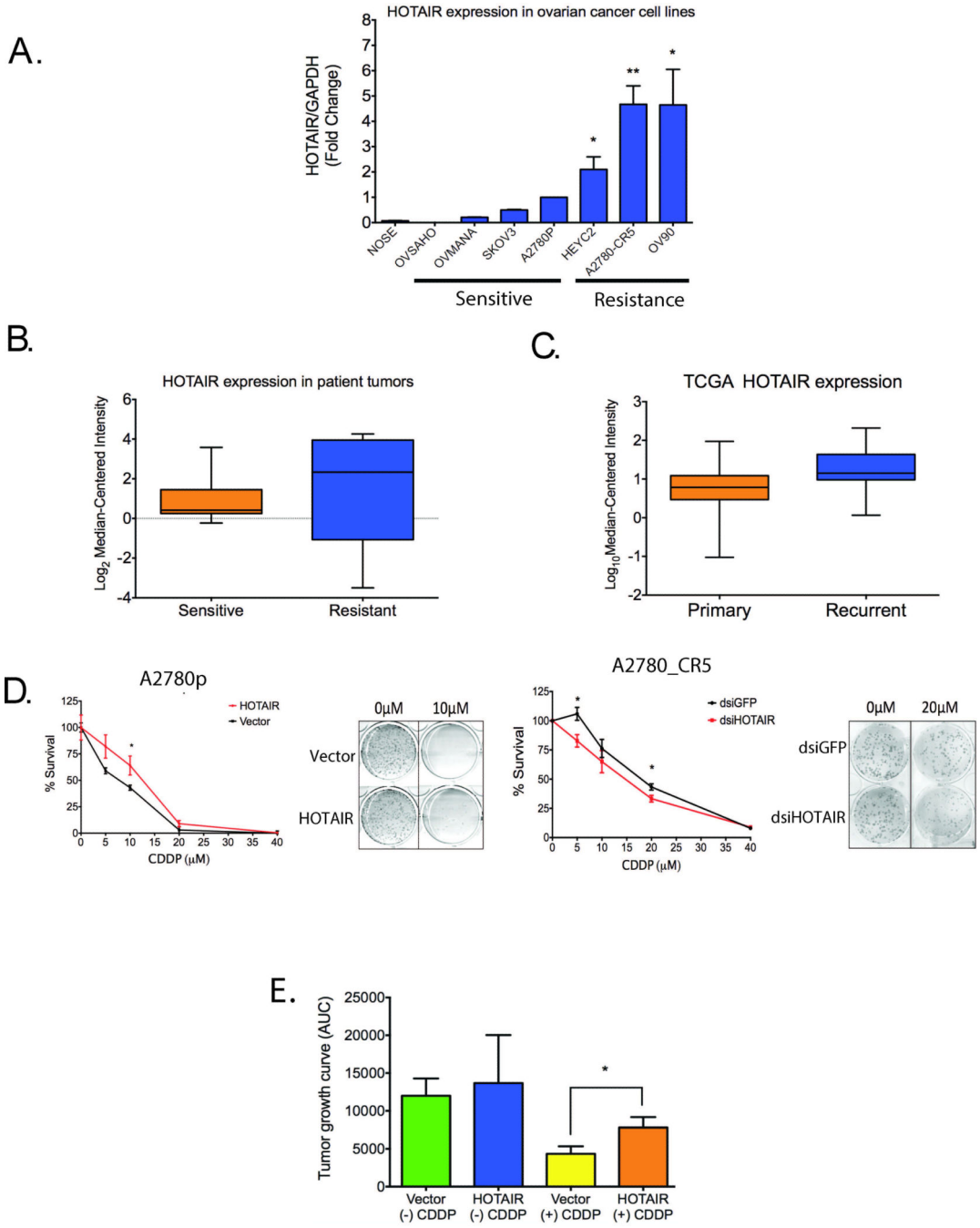

Figure 1. HOTAIR expression and characterization in ovarian cancer (OC) cells

(A) HOTAIR expression in OC cell lines (IGROV, OVSAHO, OVMUNA, SKOV3, A2780, HEYC2, A2780-CR5, and OV90) was determined by qRT-PCR, (values normalized to GAPDH). Values represent the average of three biological replicates. **(B)** HOTAIR expression in primary high-grade serous ovarian tumors from unpaired patient samples at initial diagnosis and platinum sensitive (n=11) compared to patients with recurrent and platinum resistant disease (n=14) **(C)** TCGA data analysis for HOTAIR Read Per Kilobase Million (RPKM) values in OC patients with primary vs. recurrent disease. **(D)** Clonogenic

growth in A2780p overexpressing HOTAIR (left and middle graphs) and A2780_CR5 cells with dsiRNA-mediated depletion of HOTAIR. Graphs represent the fraction of surviving cells normalized to untreated population. Graphs represent triplicate experiments. **(E)** Xenograft tumor growth in athymic mice of A2780p expressing HOTAIR and treated with cisplatin (10μM CDDP) or vehicle control (2×10^6 cells per injection). Area under the curve (AUC) was calculated at 10 weeks (n=4 mice per group). Asterisks indicate $P<0.05$ (*) or $P<0.01$ (**).

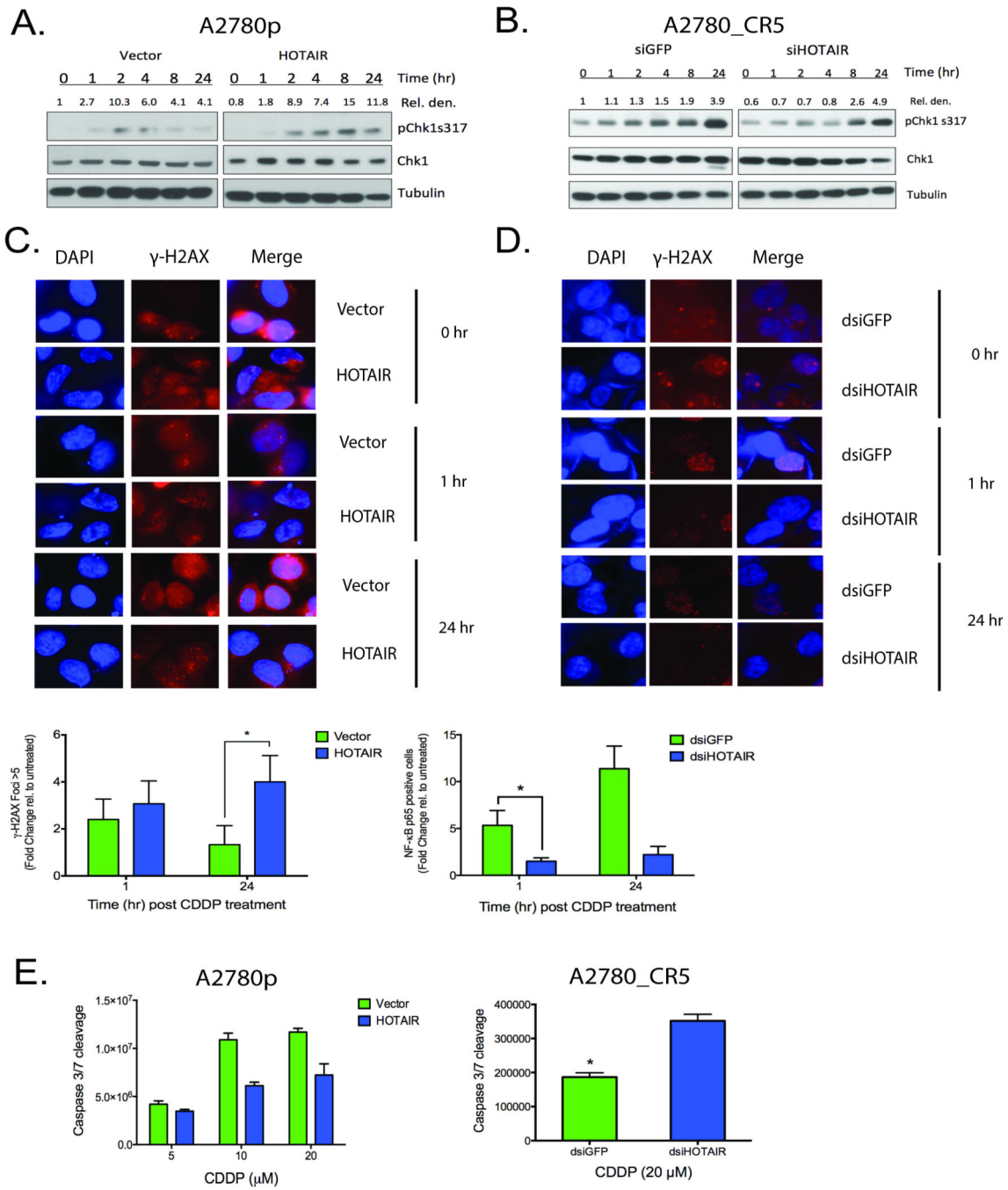

Figure 2. DNA damage induces HOTAIR expression

(A) A2780p cells transfected with HOTAIR or empty vector or **(B)** A2780_CR5 cells transfected with either dsiGFP or dsiHOT and were treated with CDDP (24 hr post-transfection). Western blots show total Chk1 and pChk1 levels at the indicated times post-CDDP treatment at the same exposure for both cell types. Western is representative of three biological replicates. **(C)** A2780p cells transfected with HOTAIR or vector control or **(D)** A2780_CR5 cells transfected with either dsiGFP or dsiHOT were untreated or treated with CDDP (10 μM). Cells were fixed and stained for γ-H2AX foci (red) at the indicated time

points. Cells were counted at 60x magnification (average of 100 cells counted) and the total number foci were determined. All experiments were repeated three times and error bars represent standard deviation (S.D.). **(E)** HOTAIR or vector expressing A2780p or A2780_CR5 cells transfected with either dsiGFP or dsiHOT were treated with indicated concentration of CDDP for 3 hrs and 24 hrs post-treatment caspase 3/7 cleavage assay was performed. Bar graph represents caspase 3/7 cleavage normalized to untreated control. Western blot is representative of two biological replicates. Asterisks indicate $P<0.05$ (*) or $P<0.01$ (**).

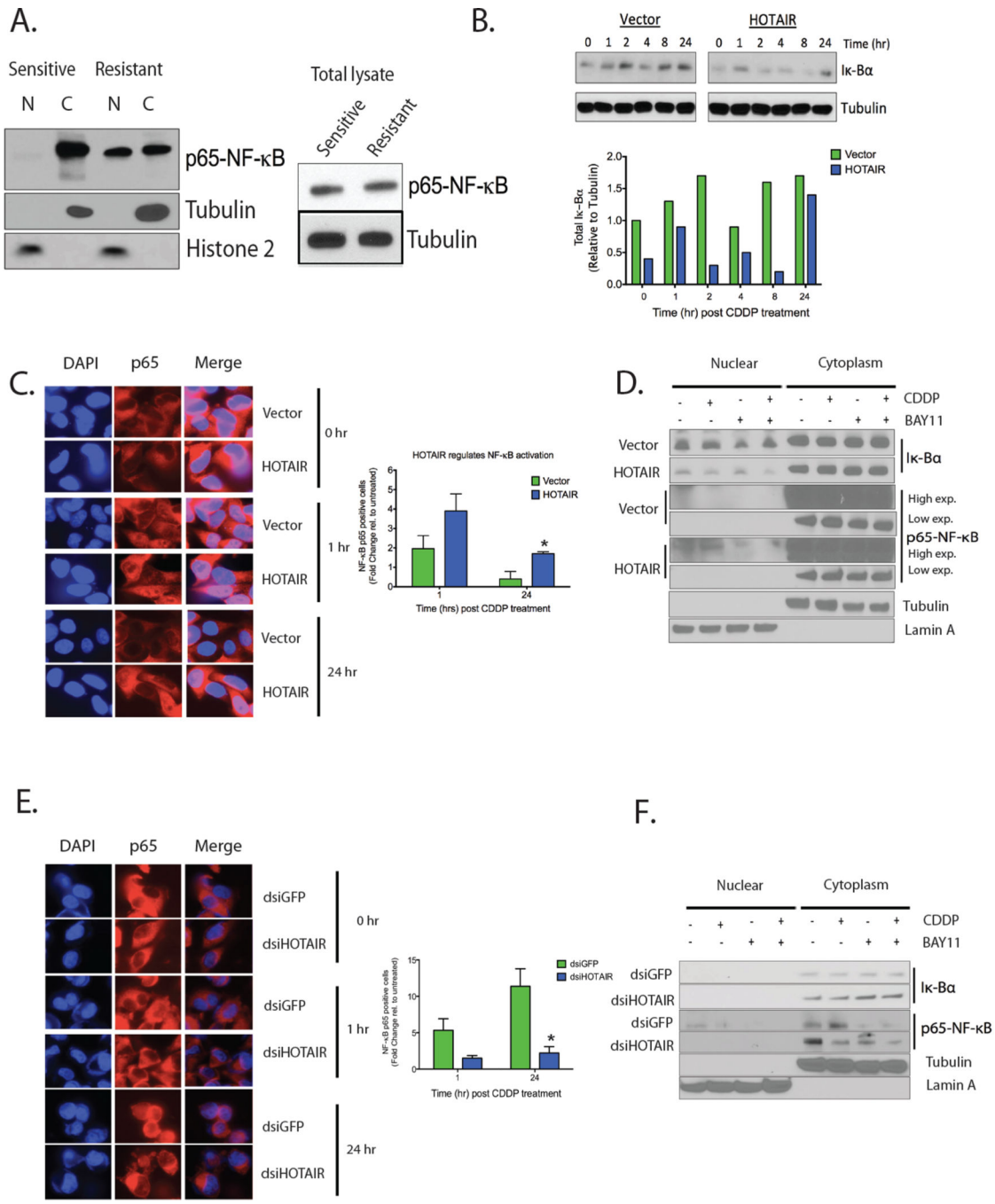

Figure 3. HOTAIR overexpression induces DDR and NF-κB target gene expression

(A) Western blot showing total Iκ-Bα and p65 NF-κB levels in cytoplasmic and nuclear fractions in A2780 and A2780-CR5 cells. **(B)** Western blot showing total Iκ-Bα levels in cells expressing vector control or HOTAIR post CDDP-treatment (10μM) at indicated times. **(C)** A2780p cells transfected with HOTAIR or vector control were untreated or treated with CDDP (10 μM) for the indicated times. Cells were fixed and stained for NF-κB p65 (red). The total number of foci was determined based on the average of 100 cells counted at 60x magnification. Bar graph represents fold change of p65 translocation relative to untreated.

All experiments were repeated three times and error bars represent standard deviation (S.D.). **(D)** Western blot showing nuclear Iκ-Bα and NF-κB levels in A2780p cells expressing vector control or HOTAIR either post CDDP (10μM), Bay-11 (3 μM) or combination treatment. **(E)** A2780_CR5 cells transfected with either dsiGFP or dsiHOTAIR were untreated or treated with CDDP (10 μM) for the indicated times. Cells were fixed and stained for NF-κB p65 (red). The total number of foci was determined based on the average of 100 cells counted at 60x magnification. **(F)** Western blot showing nuclear Iκ-Bα and NF-κB levels in A2780_CR5 transfected with either dsiGFP or dsiHOTAIR siRNA post CDDP (10μM), BAY11 (3 μM) or combination treatment.

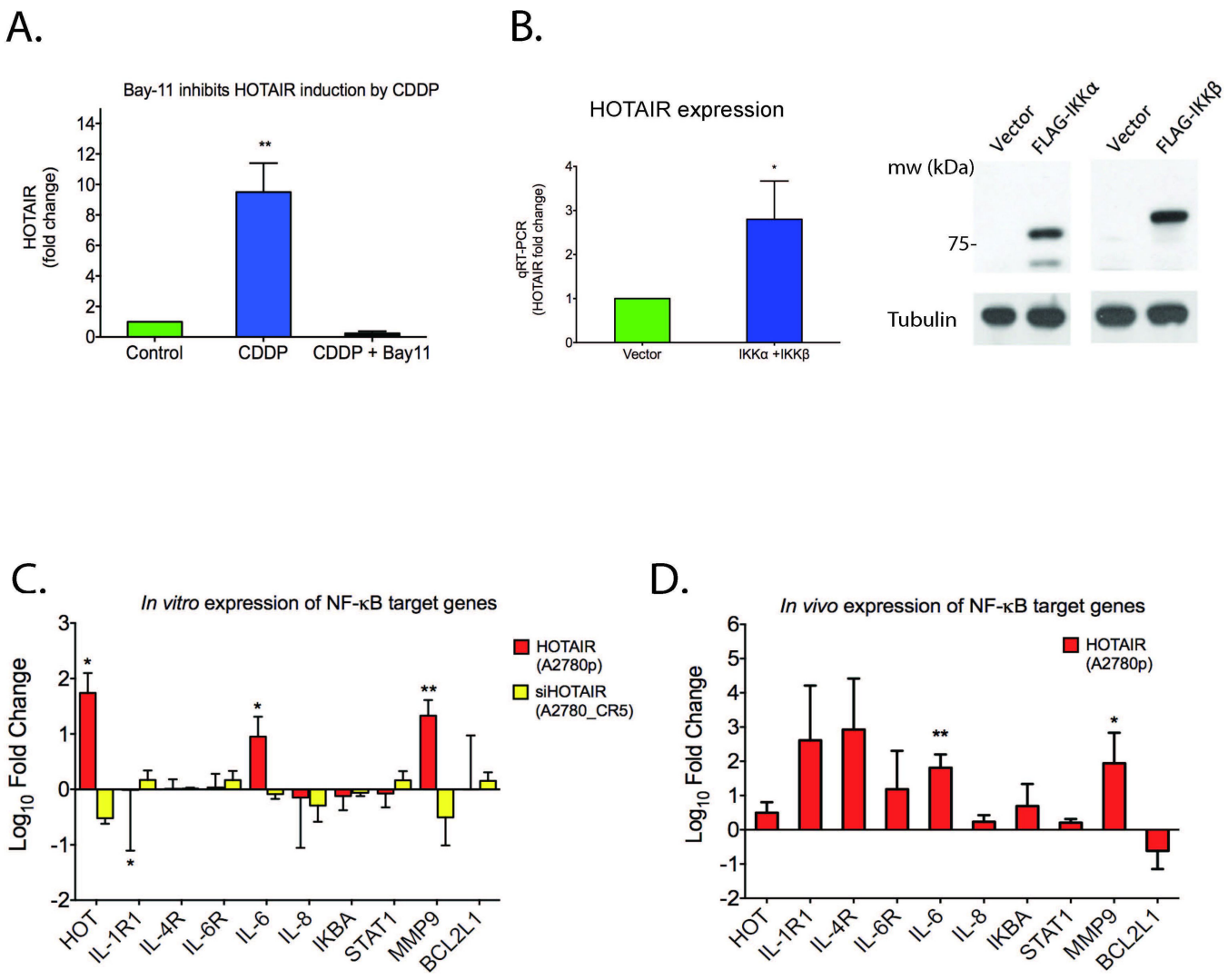

Figure 4. Transcriptional upregulation of HOTAIR by NF-κB during DNA damage

(A) HOTAIR expression in A2780p treated with CDDP alone or in combination with NF-κB inhibitor Bay-11 (HOTAIR levels measured by qRT-PCR 24hr post-treatment). **(B)** HOTAIR expression in A2780p cells transfected with IKK-α and IKK-β and western blot showing co-expression of IKKα and IKKβ in A2780p cells 24 hr post-transfection. **(C)** Average expression (log_{10} fold change) of NF-κB target genes *STAT1, IL6R, IL6, IL4R, IL8, IL1R1, BCL2L1, MMP9* in A2780p cells (red bars) HOTAIR expression (fold-change) was measured by normalizing to vector control. For A2780_CR5 cells transfected with dsiHOTAIR (yellow bars), fold change was measured by normalizing to dsiGFP transfected cells. **(D)** Average expression of NF-κB target genes measured in mouse xenografts overexpressing HOTAIR (treated with CDDP compared to untreated). Fold-change was measured by normalizing to xenografts with vector control. Bars represent average measurements +/−S.D. (n=4 per group). Asterisks indicate P<0.05 (*) or P<0.01 (**).

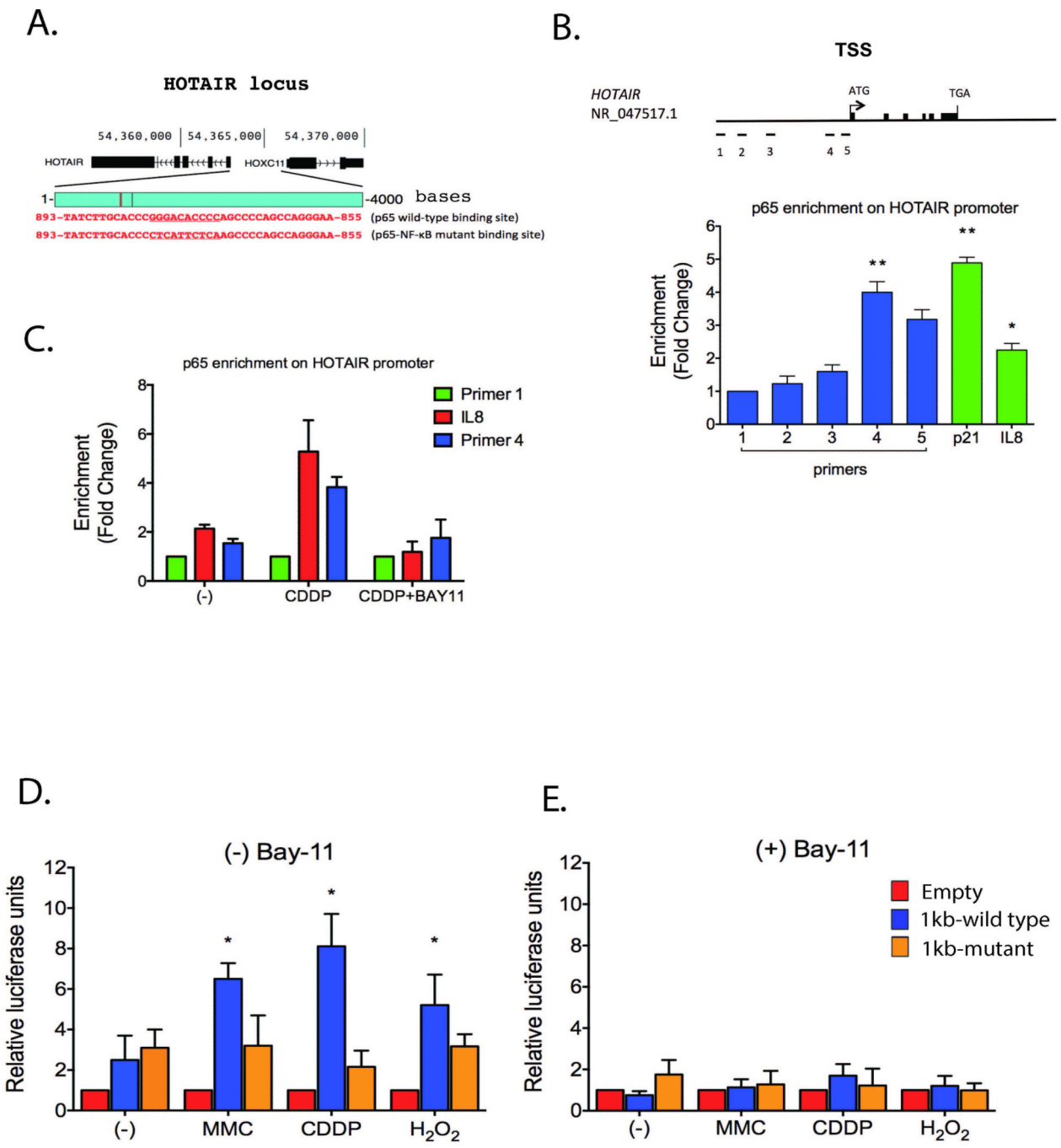

Figure 5. Direct transcriptional regulation of HOTAIR by NF-κB

(A) Map of HOTAIR promoter region showing canonical p65 binding site (908 bases upstream of TSS) and the mutant generated in PGL3 vector. **(B)** Chromatin immunoprecipitation (ChIP) in A2780_CR5 cells of NF-κB p65 targeting 5 regions upstream of HOTAIR transcription start site (TSS). (1: 10kb, 2: 8kb, 3: 5kb, 4: 908bp (consensus p65 site) and 5: 203bp). Asterisks indicate P<0.05 (*) or P<0.01 (**) **(C)** Chromatin immunoprecipitation (ChIP) in A2780_CR5 cells of NF-κB p65 post CDDP (10uM) or in combination with BAY11 (3uM) targeting regions 1 and 4 upstream of

HOTAIR transcription start site (TSS). (1: 10kb, 4: 908bp (consensus p65 site) with primer corresponding to IL8 promoter as a (+) control. **(D)** Luciferase activity of HOTAIR promoter (Illustrated in Fig. 5A) in A2780p cells treated with mitomycin C (MMC, 10μM), cisplatin (CDDP, 10μM) or hydrogen peroxide (H_2O_2, 0.5mM). **(E)** Luciferase activity of NF-κB p65 wild-type or mutant HOTAIR promoter (Fig. 4C) in A2780p cells pre-treated Bay-11 (5μM for 1 hr) then treated with MMC (10μM), CDDP (10μM) or H_2O_2 (0.5mM). Asterisks indicate $P<0.05$ (*) or $P<0.01$ (**).

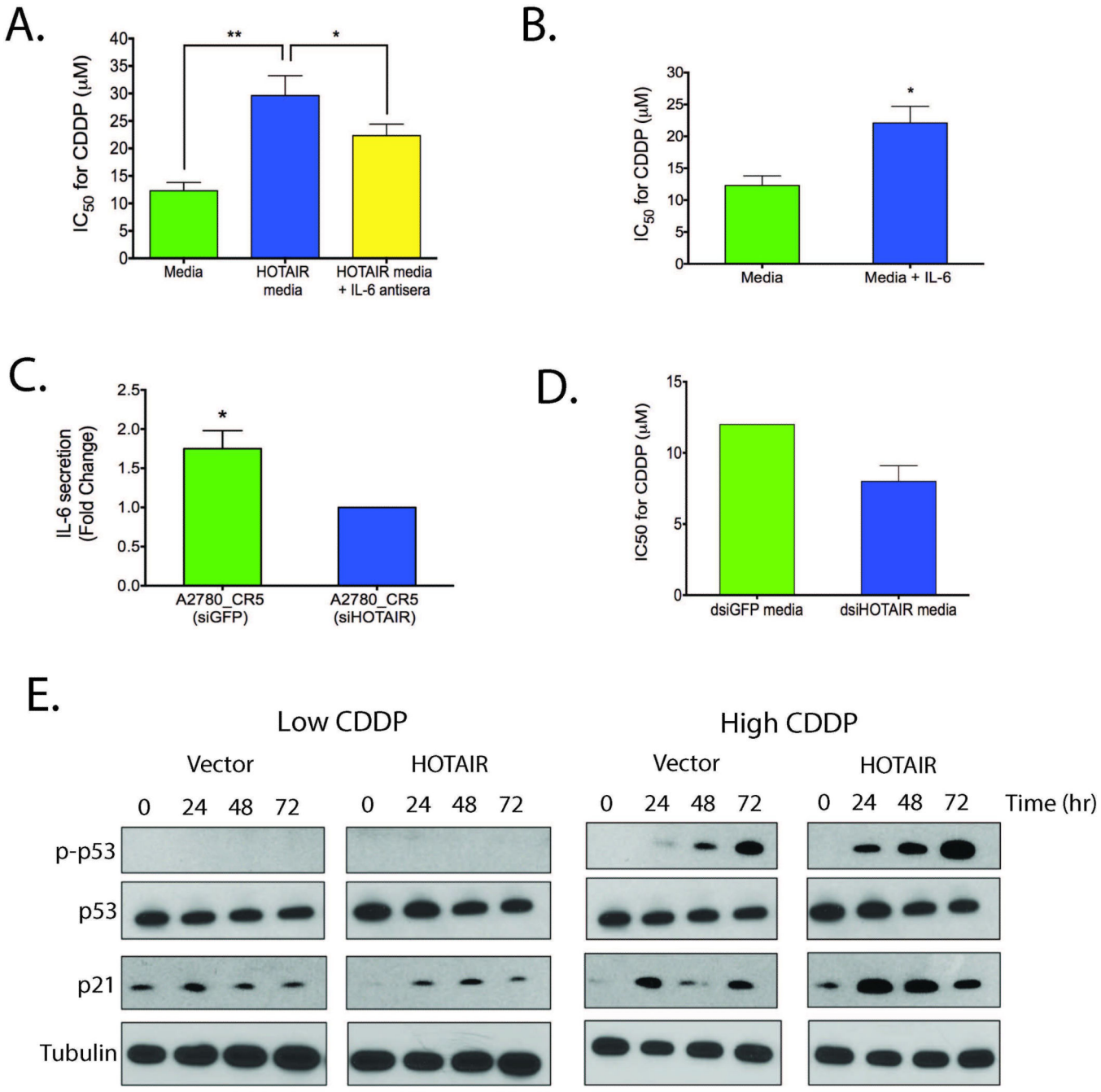

Figure 6. HOTAIR-induced IL-6 secretion

(A) HOTAIR- or control-conditioned media was added to A2780p cells and the IC_{50} for CDDP was determined by MTT assay. IL-6 neutralizing antibody was added to HOTAIR-conditioned media and IC_{50} for CDDP was compared to HOTAIR-conditioned media plus IL-6 neutralizing antibody. **(B)** Recombinant IL-6 (10 ng/mL) was added to serum-free culture media and IC_{50} for CDDP determined by MTT assay (vs. negative control). **(C)** A2780_CR5 cells transfected with dsiRNAs targeting HOTAIR was measured for IL-6 secretion 72 hr post transfection. **(D)** Conditioned media from A2780_CR5 cells transfected

with dsiRNAs targeting HOTAIR was added to cells and the IC_{50} for CDDP was determined by MTT assay. **(E)** A2780p cells transfected with HOTAIR or vector were treated with CDDP (1μM, “Low CDDP”; 20μM, “High CDDP”). Western blot analysis was performed using specific antibodies at the indicated time points. Asterisks indicate $P<0.05$ (*).

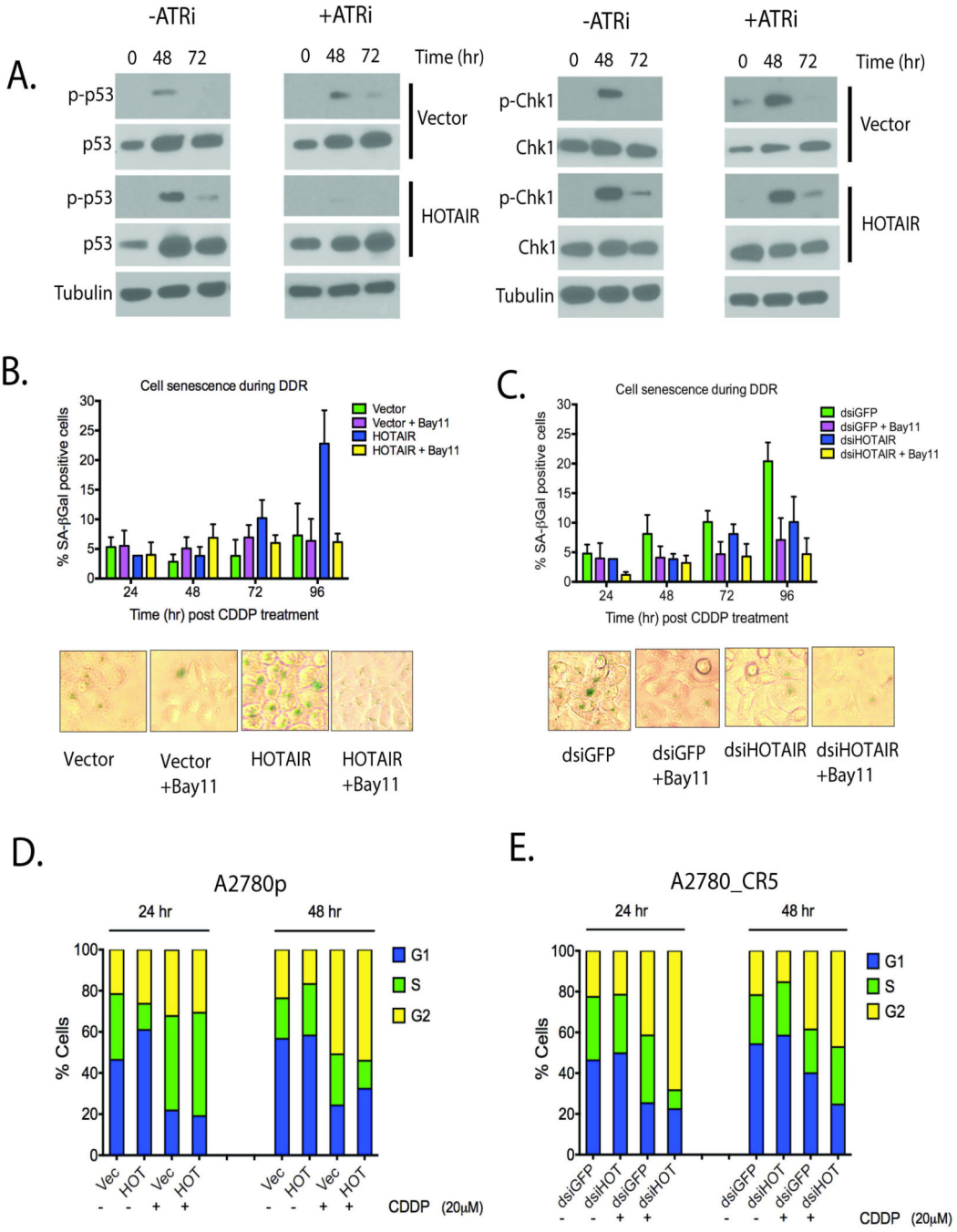

Figure 7. HOTAIR-induced cellular senescence

(A) Western blot for total p-p53 and p53 (Left) and total pChk1 or Chk1 (Right) in cells overexpressing HOTAIR or vector control with or without ATR inhibitor (5μM) followed by CDDP treatment (10μM). **(B)** HOTAIR or vector transfected A2780p cells or **(C)** dsiGFP or dsiHOTAIR transfected A2780_CR5 cells were treated with CDDP (20μM) in the presence or absence of Bay-11 (5μM) and then assayed SA-β-Gal activity to asses senescent cells. Positive cells (blue coloration) were counted at the indicated times using a microscope (20X magnification). **(D)** HOTAIR or vector was transfected in A2780 cells and 24 hr post

transfection cells were treated with 20uM CDDP for 24 or 48 hr. DNA content was measured by PI staining and flow cytometry. **(E)** A2780_CR5 cells were transfected with either dsiHOTAIR or dsiGFPand 24 hr post transfection cells were treated with 20uM CDDP for 24 or 48 hr. DNA content was measured by PI staining and flow cytometry. Asterisks indicate $P<0.05$ (*).